CEAS Space Journal (2024) 16:73–86
https://doi.org/10.1007/s12567-023-00489-w

ORIGINAL PAPER

Advanced manufacturing concept of a bio-inspired reaction wheel rotor for small- and medium-sized constellation satellites

Nils Kaiser[1] · Nils Goossens[2] · Ane Jimenez[3] · Ignacio Laraudogoitia[3,4] · Spyridon Psarras[5] · Stavros Tsantzalis[5]

Received: 28 October 2022 / Revised: 21 February 2023 / Accepted: 6 March 2023 / Published online: 30 March 2023

Abstract

The increasing number of constellation satellites requires re-thinking of the design and manufacturing process for reaction wheel rotors. Mass optimisation of reaction wheel rotors leads to cost reduction and performance increase. Those optimisations can be realised by taking ideas from nature. Therefore, design principles of diatoms were screened, abstracted and implemented in an algorithm-based design process. In this way, a bio-inspired rotor was created, which considers launch and in-operation loads, is capable of up to 7500 RPM and shows a compact design with a diameter of 282 mm. Regarding mechanical performance, an energy density of 4661 J kg^{-1} and a mass moment of inertia ratio of 0.7584, which considers the component and an idealized design, could be achieved. Compared to a commercial rotor, this is equivalent to a similar inertia ratio and +85 % energy density, but +44 % mass due to manufacturing restrictions. Based on different boundary conditions, different first natural frequency for launch and operation conditions were obtained (658 Hz and 210 Hz). The new design was cast from nano-reinforced aluminium alloy (AlSi10Mg + Al2O3) in 3D-printed sand moulds that were produced via binder-jetting process. Thus, a hybrid manufacturing process was used, by combining additive manufacturing and casting. Post-processing of the cast part via turning and milling was performed to compensate distortion and achieve the required surface quality. Preliminary vibration measurements were performed, showing a large need for balancing to achieve low vibration emissions.

Keywords Mass reduction · Optimisation · Sand casting · Vibration tests · Flywheel · Nano-reinforced aluminium

1 Introduction

Reaction wheels are actuators inside the satellite Attitude and Orbit Control System (AOCS), whose primary task is the control of the satellite orientation. The reaction wheel rotor is made of different parts and is the highest mass in the reaction wheel as shown by [1, 2]. Consequently, a rotor mass reduction would lead to a significant reaction wheel mass reduction. As [3] points out, a mass reduction by one kilogram leads to a mission cost reduction (due to reduced launch costs) of 5000€, so that even small mass reductions have a significant impact. Further, current satellite reaction wheel rotors are built from multiple parts, resulting in high assembly costs and rotor imbalance. Combining different parts to a single part as well as optimising the component shape according to the load would lead to significant imbalance reduction and wheel's system improvement.

Rotor optimisation, related to energy storage systems, is frequently discussed in the literature. [4] and [5] analysed the kinetic energy storage of different rotor geometries,

✉ Nils Kaiser
nils.kaiser@awi.de

Nils Goossens
nils.goossens@zarm.uni-bremen.de

1 Alfred Wegener Institute Helmholtz Center for Polar and Marine Research (AWI), Am Handelshafen 12, 27570 Bremerhaven, Germany

2 University Bremen, Center of Applied Space Technology and Microgravity (ZARM), Am Fallturm 2, 28359 Bremen, Germany

3 TECNALIA, Basque Research and Technology Alliance (BRTA), Mikeletegi Pasealekua, 2, 20009 Donostia-San Sebastian, Spain

4 UPV/EHU, Mechanical Engineering, Ingeniero Torres Quevedo Plaza 1, 48013 Bilbao, Basque Country, Spain

5 Department of Mechanical and Aeronautical Engineering, University of Patras, Applied Mechanics Laboratory, Rio, 26500 Patras, Greece

whereas [6] presented a novel approach for shape optimisation using the evolutive system method. Further works dealt with a numerical shape optimisation based on even stress distribution [7], a topology optimisation based approach for maximising energy density [8] or a shape optimisation approach using parametric geometry modelling for maximising energy density [9]. Additionally, [10] analysed the optimal shape, size and material of rotors with respect to maximum kinetic energy. As extensive as the literature for energy storage systems is in general, as limited is it with respect to rotor optimisations for satellite reaction wheels. [11] discussed an axis-symmetric topology optimisation of a reaction wheel rotor for an earth observation mission.

One way to improve technical components is the imitation and implementation of principles found in nature. In this sense, a bio-inspired design is the combination of solutions from nature and technology, aiming for an improved design by getting inspired by instead of copying nature [12]. The motivation behind this transfer is the diversity of nature, which offers a great source of inspiration [13], and the evolution, in which over the course of 3.8 billion years biological structures have been optimised [14]. If organisms have a higher chance of survival compared to others due to lightweight structures, the resulting constructions come very close to an optimal lightweight solution due to improvement over million of years [15].

Such an example is represented by diatoms, marine microorganisms of a few µm to a few mm in size that occur in more than 100–000 species with different forms and sizes [16], as shown in Fig. 1. Their shells are optimised for stiffness and lightweight design and exhibit a high degree of symmetry, complexity and self-similarity [17]. In this way, they are able to protect themselves from predators and to float in the upper water depths, which is essential for their survival [18].

Due to their diversity, different design principles of diatoms have been applied in various technical fields. There were studies in the automotive sector on plastic deformation elements [20] or developments of A-pillar reinforcements [21], a concept for an offshore foundation structure [22], studies on the influence on natural frequency [23, 24] and the improvement of a girder structure [25]. Furthermore, a holistic lightweight design optimisation process that harnesses appropriate lightweight design principles to develop engineered components was developed by [26].

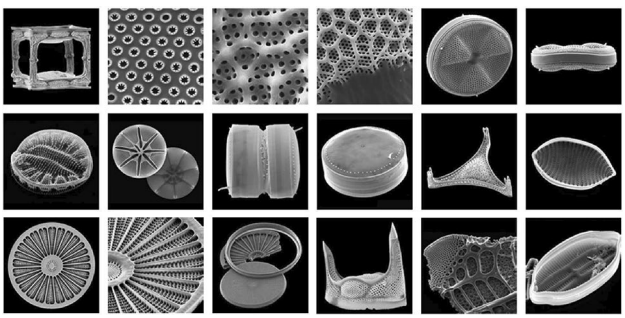

Fig. 1 Scanning electron microscope (SEM) images of diatom shells (modified according to [19])

The advanced manufacturing process applied in the presented work is a hybrid method based on casting and 3D-printing. Using additive manufacturing for the production of the mould and an aluminium casting process for expendable moulds as the main manufacturing process, higher geometric complexity and being cost effective at the same time is achievable. Compared to industries where expendable moulds were not efficient because of the required number of parts, in space industry expendable moulds are suitable regardless of the increased number of satellites launched because the mass restrictions outweigh the number of parts needed.

The objective of the present work is to describe a development process of a mass-optimised, single-part reaction wheel rotor with a bio-inspired design, made by advanced manufacturing and used in small to medium satellites, since the satellites size shifts towards this direction as they are frequently used in satellite constellations [27].

The presented work was part of LOBSTER, a 6-month subproject conducted in the framework of the EU-funded project OASIS (**O**pen **A**ccess **S**ingle entry point for scale-up of **I**nnovative **S**mart lightweight composite materials and components), which included the manufacturing of a demonstrator and first simplified analysis to identify potential for further studies.

The paper is structured as follows: Chapter 2 describes the constraints for the reaction wheel rotor which are the baseline for the bio-inspired design process presented in chapter 3. Chapter 4 addresses the advanced manufacturing process of nano-reinforced aluminium casting with 3D printed casting moulds, followed by functional testing in chapter 5. The discussion of the obtained results is given in chapter 6, while chapter 7 concludes with a summary of key findings.

2 Application constraints

The present work focuses on the development of a mass-optimised, fast spinning (up to 7500 RPM) reaction wheel rotor with a maximum radius of 300 mm and a mass moment of inertia between 0.051 kg m^{-2} to 0.06 kg m^{-2}, leading to a momentum storage capacity of at least 30 N m s. Rotors with similar inertia and momentum storage capacity can be made of stainless steel A316 or polymer PEEK and can have a mass of about 2.3 kg, but at the same time require larger diameters (about 350 mm) and lower rotational speeds

(4500–6000 RPM) [1, 11]. According to [28], such rotors can be used for small- to medium-sized satellites.

In contrast to common reaction wheel rotors, the new design is made of nano-reinforced aluminium. By this decision, demisability—the breaking melting of parts during re-entry which lowers the risk of harming anything on the ground—is taken into account. Stainless steel rotors have a higher chance to survive or only partially ablate during re-entry [1] and the use of aluminium in reaction wheel rotors can help to improve this aspect [29]. In addition, aluminium rotors have higher specific energy density at lower rotor radii and high speeds compared to steel rotors [10], which is in line with a reaction wheel for small- to medium-sized satellites.

To enable the use of nano-reinforced aluminum, casting is chosen as manufacturing process. In addition, manufacturing by casting can satisfy small-scale serial productions associated with the increasing demand for small- and medium-sized satellites and at the same time, provide complex shapes like it can been seen in mass optimised parts.

Regarding mechanical performance of the rotor, the considered load conditions are differentiated into launch and in-orbit operation, which are related to different loads, boundary conditions and minimum first natural frequency requirements. To allow fast development, the mechanical calculations are simplified and explained in detail in chapter 3.3. As the focus is on the rotor design, additional rotor elements like ball-bearings, the motor and locks, are considered as simplified geometries based on commercial components.

3 Bio-inspired design process

The bio-inspired design process was applied to optimise a rotor design. Using design principles found in nature, an optimal mass distribution should be created, which incorporates mass reduced structures, is highly adapted to defined loads and generates the mass moment of inertia with least amount of material. To develop the design, bio-inspired design principles were used in a generative, algorithm-based workflow. Adapted from the problem-driven bio-inspired design approach of [30] and the technology pull method of [31], different steps like problem definition, search for biological role models and implementation of abstracted principles were conducted. Accordingly, the development process of the design was divided into different steps, which are shown in Fig. 2 and explained in the next chapters.

For the creation of the design, the software Synera (Synera GmbH, Bremen, Germany) was used, which enables the development of complex CAE models, based on an automated and algorithm-based development process. For topology optimisation, the software Altair HyperMesh in combination with the OptiStruct solver (Altair Engineering Inc, Michigan, USA) was used.

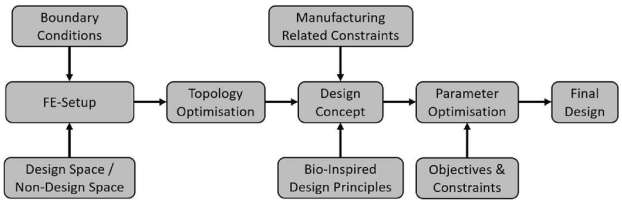

Fig. 2 Workflow of the bio-inspired rotor design creation

3.1 Problem definition

For the technical problem of a mass optimization of a rotor, solutions were searched for in different diatoms. The problem was described with Eq. (1) whereby all values were depended from the parametric rotor design, whose parameters are given in Table 1 in Sect. 3.6.

$$\min_{\text{rotor design}} \begin{Bmatrix} m_{\text{ro}} \\ -I_{\text{ro}} \\ -F_{\text{n,l}} \\ -F_{\text{n,o}} \\ -I_{\text{rat}} \\ -L \\ \sigma_{\text{y}} \\ d_{\text{max}} \end{Bmatrix} \tag{1}$$

with the constraints

$$\begin{aligned} 0.051\,\text{kg m}^{-2} \leq I_{rotor} &\leq 0.06\,\text{kg m}^{-2} \\ F_{\text{n,l}} &\geq 150\,\text{Hz} \\ F_{\text{n,o}} &\geq 190\,\text{Hz} \\ L &\geq 30\,\text{N m s} \end{aligned}$$

m_{ro} Rotor mass

I_{ro} Rotor mass moment of inertia

$F_{\text{n,l}}$ First natural frequency for launch boundary conditions

$F_{\text{n,o}}$ First natural frequency for in-operation boundary conditions

I_{rat} Inertia ratio (see Sect. 3.6)

L angular momentum (see Sect. 3.7)

σ_y Yield strength

d_{max} Maximum displacement

3.2 Design space

The maximum available space for the new rotor was a cylinder, which is 150 mm in height and 300 mm in diameter. The design of the new rotor was based on the assumption, that the rim, the outer most part of the rotor, is mainly responsible for the generation of mass moment of inertia. The remaining rotor material has a small impact on the inertia. Furthermore, the rim could be seen as a ring for the calculation of its mass m_{ring} and mass moment of inertia I_{ring}.

$$m_{ring} = h_{ring} \cdot \pi \cdot \rho \cdot (r_a^2 - r_i^2) \tag{2}$$

$$I_{ring} = 0.5 \cdot m_{ring} \cdot (r_a^2 + r_i^2) \tag{3}$$

ρ Density of aluminium

r_i Inner radius of the ring

r_a Outer radius of the ring

The height of the ring h_{ring} was equal to the maximum height of the design space with 150 mm. Considering the maximum diameter, the rim width can be calculated by substituting Eq. 2 in Eq. 3, rearranging to r_i and assuming that the rim inertia should be equal to the minimum requested mass moment of inertia.

3.3 Load cases and boundary conditions

The rotor must be able to withstand the loads during operation in-orbit as part of a satellite and additionally during transport to space. Therefore, two different load and boundary conditions were considered as these are in no way similar. The assumed load amplitudes and frequency have been average values for earth observation mission given by the industry partner.

While launching, the rotor experiences dynamic loads caused by the launchers. Using the Miles equation, those loads were simplified into acceleration loads of 20 g, separately applied in X-, Y- and Z-direction. The rotor is fixed to the inner surfaces of the connection elements, which is equivalent to being secured at launch by launch locks. The mounting points for the launch differ from the operational mode. The launch lock position is selected in such a way that the rotor has a minimum loading. To avoid critical vibrations, the first natural frequency at launch should be greater than 150 Hz.

For in-orbit operation, the main load is based on centrifugal forces, which were generated due to the maximum rotational speed of 7500 RPM around the vertical Z-axis. In addition, a disturbance torque of 3.56 Nm was applied separately about the horizontal X- or Y-axes. This disturbance was present due to an assumed satellites slew and coupled imbalance, taking into account a safety factor of 1.5. The satellite slew ω_{slew} is defined as 1 degree per second, resulting in a gyroscopic torque of 0.52 Nm for the given rotational speed and required angular momentum:

$$\tau_{gyro} = \omega_{slew} \cdot L \tag{4}$$

A value of 30 gcm^2 is assumed for the coupled imbalance. Multiplied with the rotational speed, a value of 1.85 Nm was considered as part of the disturbance torque. Boundary conditions were assumed to be fixed at the rotor surfaces in contact with the bearings, changing the required minimum natural frequency to 190 Hz for the in-orbit condition.

In total, 3 different static load cases for launch and 2 for operation conditions were considered.

3.4 Topology optimisation

Topology optimisations were carried out to identify the load-bearing areas common for all load cases. These provided the basis for the new design. As defined before, the rim was mainly responsible for the mass moment of inertia, so that it remained solid and unaffected by the topology optimisation (non-design space). In addition, a simplified structure at the center of the rotor, which is used to cover and attach wheel components like ball-bearings and the motor, was defined as a second non-design space; the third were three connection elements for lock applications. All non-design spaces are shown blue-highlighted in Fig. 3a, while the design space, which remains when non-design spaces and spaces required for additional wheel components are subtracted from the available space, is presented in grey.

The nano-reinforced aluminium alloy AlSi10Mg + Al2O3 used for the rotor simulation had a density of 2.6 t m^{-3}, a yield strength of 0.08 GPa, a Poisson ratio of 0.33 and a Young's modulus of 71.5 GPa. Due to the given rotational symmetry, a rotational symmetry criterion was activated for the optimisation, with the aim of generating a new design by rotating identical cylinder sectors (analogous to circle sector). Two different settings were considered, 3 or 6 sections. Both setups were complemented by a minimise weighted compliance objective considering all load cases equally weighted with a factor of 1, and constraints for a volume fraction of 0.2 as well as minimum first natural frequencies.

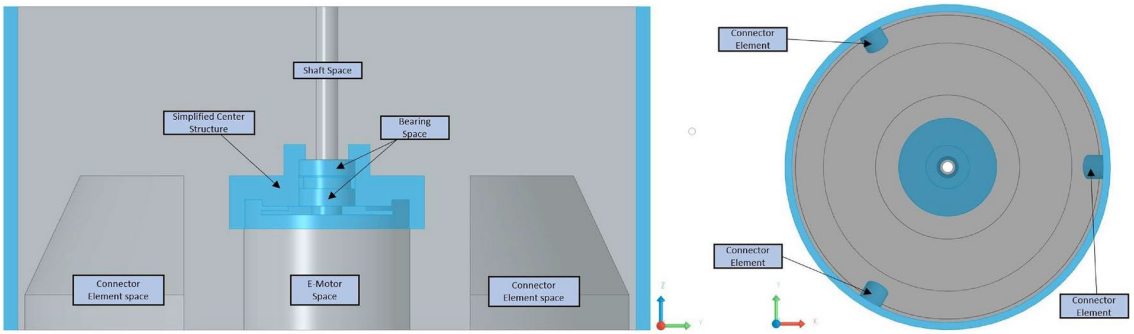

(a) *Cross-section and top-view of the design space (grey) and non-design space (blue) used for the topology optimisation.*

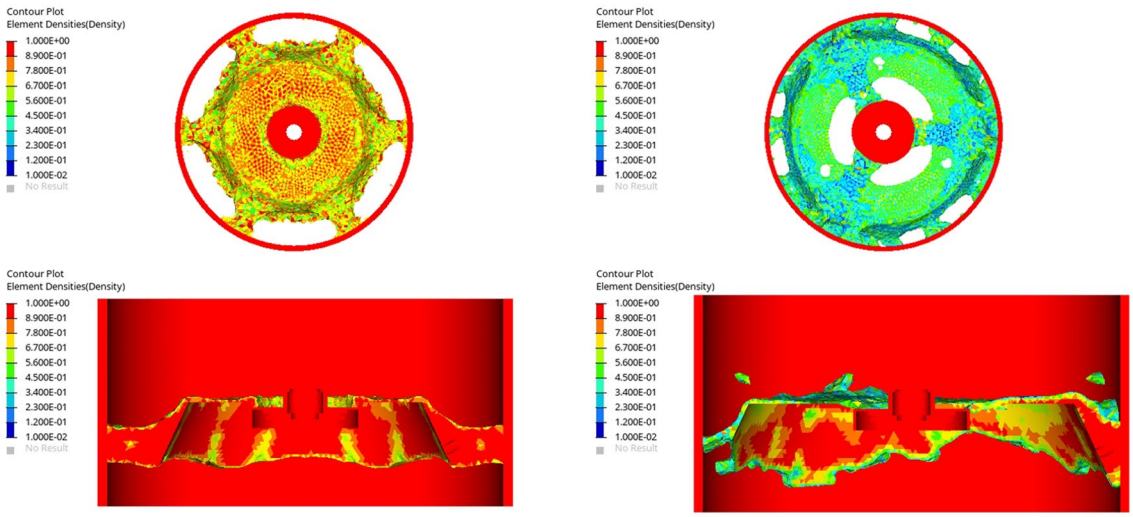

(b) *Topology optimisation results using 6 (left) or 3 (right) rotational symmetric cylinder sectors.*

Fig. 3 Design spaces and topology optimisation results

Due to the different boundary conditions, the frequencies differ between launch (150 Hz) and operation (190 Hz). The results of the optimisation are shown in Fig. 3b.

3.5 Analogy search and biological templates

To be able to create a preliminary bio-inspired design of a rotor, biological models had to be selected in a first step, which were abstracted to bio-inspired structures in the following step. For this purpose, analogies were defined, which were used to search the literature and databases for suitable diatom species and design principles of their shells. Analogies could refer to entire organisms or to specific features of individual areas of the shells. The considered analogies corresponded to three different fields: Function, Requirement and Form. While the analogies for the first two fields resulted directly from the specifications for the new component, the third field was derived from the design of the topology optimisation results (Fig. 3b), which allowed the load-bearing areas to be considered for the new design.

Accordingly, the rotor should be built from rotational symmetric cylinder sectors. The central area should consist of a few, stronger struts with large, trapezoidal cavities. The main area of the rotor contained flat structures possibly reinforced with rib structures. Alternatively, comb-like or lattice structures could replace those structures to improve lightweight. Although only partially visible in the results, a mirror symmetry with respect to the horizontal was assumed to reduce design-related imbalance. In summary, the analogies were defined as:

- Function: Mass concentration in outer areas, loading due to rotation, loading due to acceleration
- Requirement: Load transfer and distribution from center to outside, areas with less or no mass, connection structures with low mass, combination of load carrying and load transferring sections, smooth connections

– Form Cylindrical, rotational symmetry, struts and cut-outs, flat structures, horizontal symmetry

3.6 Design concept and bio-inspired rotor design

According to the biological role models, bio-inspired structures were generated, combined with the non-design space of topology optimisation to form a preliminary parametric design, and then optimised. As can be seen in the schematically-displayed right half of the new design in Fig. 4, a two-part, radially-symmetric structure similar to the shell shape of *Asterolampra marylandica* and *Rocella schraderi*, was derived. Analogous to the models, the centrally located area contained larger structures. The outer part was formed by regular, comb-like structures, whose size increased towards the outside and can be found in different forms in diatoms (e.g. *Thalassiosira sp.*). Due to rounding of the comb-like pattern and thickening of the ribs running between them, the comb-like structures were hardly recognizable as such in the final design. Instead, the outer area was derived into a ring with irregularly shaped oval cavities. The ribs emerged from much thicker structures in the rotor center and split outward, allowing loads to be directed and distributed from the center to the outer areas. In addition, smooth or rounded transitions and varying structural thicknesses are found throughout the design, in keeping with the biological role models.

To achieve the optimal setting and combination of the bio-inspired design principles, an automated parameter optimisation was performed using the MIDACO solver (Mixed Integer Distributed Ant Colony Optimisation). This solver implements a derivative-free, evolutionary hybrid algorithm and can be used for single- and multi-objective optimisation with up to thousands of variables and hundreds of objectives [33]. In this way, for example, the number and arrangement of the comb-like structures or the strengthening of their fillets or sizes was adjusted, so that the structures were adapted according to present loads. FEM simulations were performed for every new design to ensure compliance with stress values lower than yield strength. An overview about all parameters used, is given in Fig. 5 and table 1. The optimization objectives were set according to Eq. (1) in chapter 3.1.

Through the parametric design and the algorithm-based design environment in Synera software, manufacturing-relevant design constraints could be integrated into the development process based on logic and mathematical rules to enable manufacturability. In this way, fillets of at least 3 mm for each edge were applied and a minimum material thickness of 7 mm was guaranteed. Furthermore, massive solid areas were avoided and transitions between different structures have been smoothed. Due to the minimum thickness, designs based on lattice structures or rib reinforced surface structures had to be excluded. The final design of the rotor shown from different perspectives is presented in Fig. 6.

The inertia ratio, given here as figure of merit, described the proportion between the inertia of the new rotor I_{ro} and the inertia of an idealised ring I_{ideal}, where all mass is located on the radius.

$$I_{rat} = \frac{I_{ro}}{I_{ideal}} = \frac{I_{ro}}{m_{ro}} \cdot r_a^2. \tag{5}$$

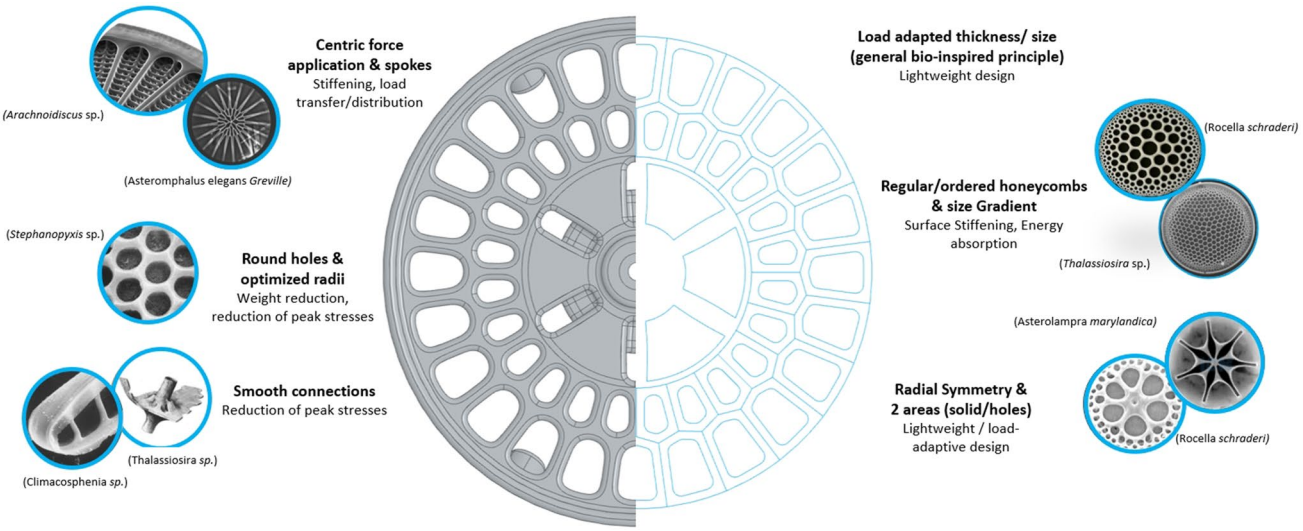

Fig. 4 Final design of the rotor in a rendered (left) and schematic (right) representation, including an overview about the marine microorganisms used to abstract bio-inspired design principles and structures (modified according to [16, 32])

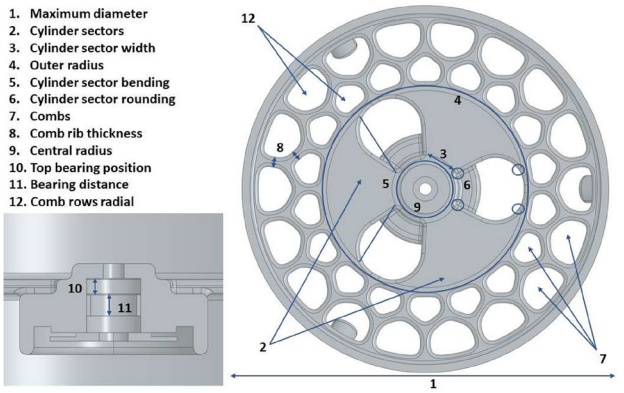

Fig. 5 Visual representation of the adaptable parameters for the parameter optimisation based on a preliminary design

3.7 Performance of the new rotor

To comment on the performance and potential of the new rotor design, comparative data from a commercially used rotor (RSI25-220/45 from Rockwell Collins Inc., Cedar Rapids, Iowa, USA) and a conceptual, topology-optimised rotor design [11] were used. Since no data was available for the wheel of the commercial reaction wheel rotor, a simplified rotor with comparable properties based on data from [1] was used. In addition to the rotor properties already mentioned, the inertia to mass ratio I_m, the angular momentum L and the energy density e as kinetic energy E_{kin} to rotor mass ratio were considered for the performance evaluation, calculated based on the CAD-model.

$$I_m = \frac{I_{ro}}{m_{ro}} \tag{6}$$

$$L = I_{ro} \cdot \omega \tag{7}$$

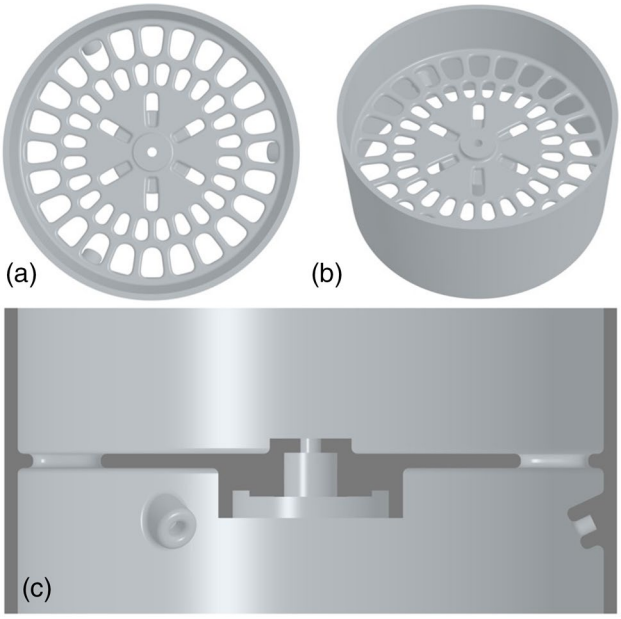

Fig. 6 Final design of the bio-inspired rotor shown from top (**a**), perspective (**b**) and cross-sectional view (**c**)

$$e = \frac{E_{kin}}{m_{ro}} = \frac{0.5 \cdot I_{ro} \cdot \omega^2}{m_{ro}}. \tag{8}$$

The bio-inspired rotor had a diameter of 282 mm and a maximum rim height of 150 mm, while possessing a mass of 3.375 kg. The moment of inertia was 0.051 kg m^2 and the inertia ratio was 0.7528, resulting in an inertia to mass ratio of 0.0151 m^2. With a rotational speed of 7500 RPM, the rotor showed an angular momentum of 40 N m s and a energy density of 4661 J kg^{-1}. Corresponding values were generated for the commercial and conceptual reference models. All values are summarised in table 2. Compared to the reference

Table 1 Parameters of the parameter optimisation

#	Parameter	Range	Definition	Explanation
1	Maximum diameter	280–300 mm	Absolute	Lower bound due to launch locks and requested moment of inertia
2	Cylinder sectors	3 or 6	Absolute	Number of structures in the center area
3	Cylinder sector width	0–1	Relative	0 represents a width of 14 mm and 1 the maximum possible width
4	Outer radius	0.1–0.8	Relative	Radius of the inside structure in relation to the maximum possible radius
5	Cylinder sector bending	0–1	Relative	0 is related to "straight" and 1 to the maximum bending
6	Cylinder sector rounding	1.5–3 mm	Absolute	Fillet radius for rounding vertical edges of inner structures
7	Combs	12, 18 or 24	Absolute	Number of combs within one row
8	Comb rib thickness	3.5 - 5 mm	Absolute	Rib thickness between different honeycombs
9	Central radius	23 - 45.2 mm	Absolute	Based on the size of the non-design space
10	Top bearing position	− 11 to 64	Absolute	Z coordinate of the upper bearing center of gravity
11	Bearing distance	0–1	Relative	0 is related to no distance, and 1 represents the maximum distance
12	Comb rows radial	2, 3 or 4	Absolute	Number of combs in radial direction

Table 2 CAD-model based reaction wheel rotor performance of the bio-inspired design, a simplified commercial design [1] and a conceptual design [11]. Improved values of the new design are written in bold and less-performable values are underlined

Rotor	Diameter [mm]	Rim height [mm]	Mass [kg]	Inertia [kg m^2]	Inertia to mass ratio [m^2]	Inertia ratio [-]	Energy density [J kg^{-1}]	Angular momentum [N m s]	RPM
Concept	350	93	2.24	0.041	0.0183	0.5971	3610	26	6000
Commercial	347	99.2	2.34	0.053	0.0227	0.7532	2517	25	4500
Bio-inspired	**282**	**150**	3.375	0.051	0.0151	**0.7584**	**4661**	**40**	**7500**

models, improved values of the new design are written in bold and less-performable values are underlined.

Regarding first natural frequency, the new design for the start condition possessed 658 Hz, well above the required 150 Hz. In operation, the first natural frequency was 210 Hz and thus also above the required value of 190 Hz. The maximum occurring stress was about 18 % below the yield strength criteria of 53.3 MPa, based on a safety factor of 1.5. The safety factor is obtained by multiplying a parameter for consideration of metallic parts with critical yield strength (1.25) [34] and an additional parameter (1.2) that takes into account the coarse manufacturing tolerances of a casting manufacturing process [35].

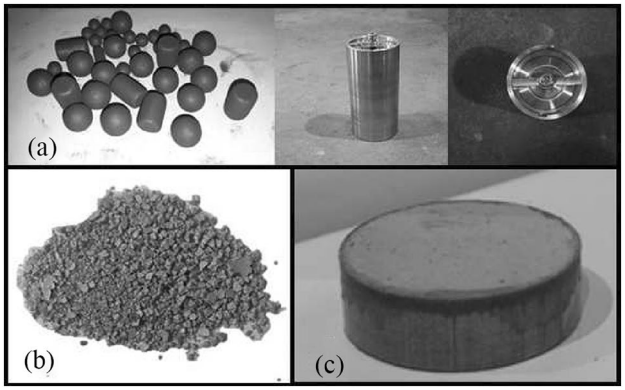

Fig. 7 The milling process from raw material to pellets. **a** Raw material (left) and the canister in which the raw material is introduced and milled. **b** Milled material in the needed particle size. **c** A pellet made of nanoparticles by pressurising them into a cylindrical shape

4 Advanced manufacturing

The manufacturing process started with the material preparation 4.1, followed by the process modelling and an enhancement of the design with casting specific elements 4.2. The generation of the mould 4.3 was the next step, while manufacturing and post-processing of the new design were the last steps 4.4.

4.1 Material preparation

Ball milling was the first phase of the particle preparation process. In this way, the aluminium coat the nanoparticles to facilitate the incorporation of the nanoparticles into the molten matrix [36]. The ball milling process was carried by rotating a canister filled with aluminium powder, steel balls and ceramic nanoparticles (Fig. 7a) on a constant speed. Due to collision with the steel balls and a rotating duration for 24–48 h, a homogeneous mixture of ceramic particles and aluminium powder was obtained, shown in Fig. 7b. In the following pressing phase, aluminium-coated ceramic nanoparticles were pressed with loads between 2-7 tons. In this way, the loose material was transferred into a compact shape, called pellet, which is more suitable for further processing (Fig. 7c).

For the casting process of the rotor, ingots made of nano-reinforced Aluminium were needed. Therefore, the stir casting process according to [37] was used. AlSi10Mg alloy was melted in a silicon carbide crucible in an electric resistance furnace by reaching a furnace temperature of up to 700−740° C. Once the material was melted, a stirrer was introduced to generate a vortex, Al2O3 nanoparticles were introduced and the stirring was maintained for 15 min. Finally, the melt was cooled down to 700−720° C and poured in a metallic die.

4.2 Casting design

The manufacturing method chosen to build this part was gravity casting in sand due to the complexity of the geometry. To facilitate filling the axially symmetrical part, the mould rotated while pouring the metal. To perform the casting in a correct way, an adequate filling system had to be designed, which conduct the liquid material through the mould cavities. The filling system depends on the orientation of the part. Three different orientations could be considered in this case (see Fig. 8). Since the part must be filled homogeneously throughout the radius to avoid excessive axial unbalance, orientation C was discarded. If the part would be filled from the outside (orientation A), it would be necessary to add several points of attack so the post-processing could lead to more axial unbalance and would be more complex due to removal of flutes and

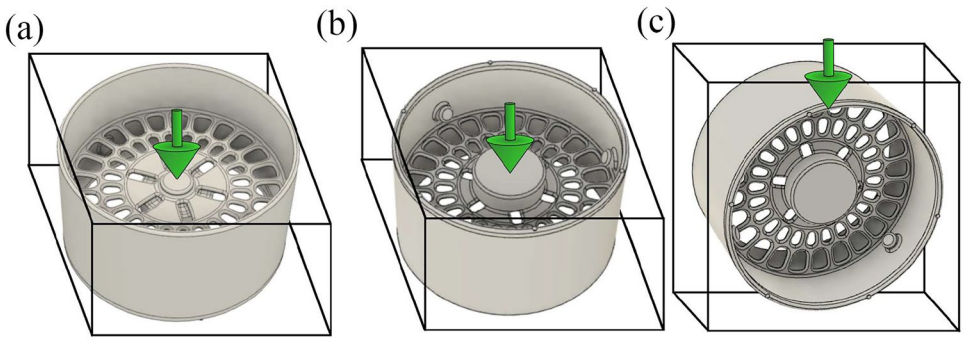

Fig. 8 Three orientations possible for filling the part. **a** Filling in horizontal upwards. **b** Filling in horizontal downwards and **c** filling in vertical

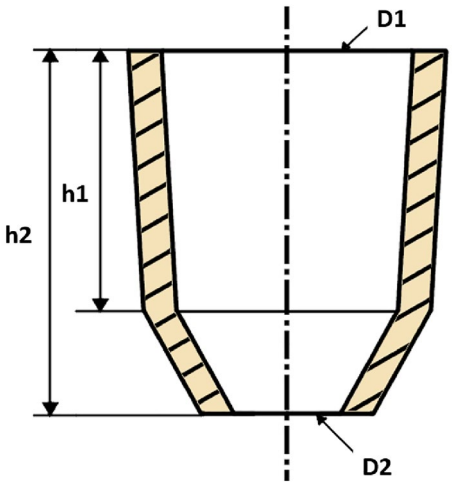

Fig. 9 Geometric parameters for commercial feeder selection. In the present case $D2$ is 70 mm, $D1$ is 152 mm, $h1$ is 126 mm and $h2$ is 181 mm

hit points in a circular geometry. For filling from the inside (orientation B), a large feeder in the center is required to feed the entire part before starting to solidify and risers might be needed on the outside to avoid defects in the bumps. Because of more usable area to place a larger feeder and less complex post-processing, orientation B was selected.

The feeder had to be dimensioned so that the feeding system ensured good control of the melt flow without splashes or impacts, avoid dragging impurities, be able to fill the part correctly and be easy to disassemble. Based on the surfaces that houses the electric motor, which is where the feeder was placed, the channel had a maximum size of 84 mm. Corresponding to the feeder shape shown in Fig. 9, a commercial feeder from the Company FOSECO with 70 mm diameter $D2$, 152 mm diameter $D1$, 126 mm height $h1$ and 181 mm height $h2$ was chosen.

Three risers were used to feed the parts during the solidification period, to compensate the metal shrinkage and to avoid the formation of porosity in the parts. To dimension the risers, the solidification time t must be calculated using Chvorinov's rule [38]. In sand casting, the mould material controls the rate of heat loss during casting, so that the following equations can be used to determine t and the mould coefficient B.

$$t = \frac{\pi}{16 \cdot K_m \cdot \rho_m \cdot C_m} \cdot \left[\frac{a \cdot \rho_s \cdot H}{(T_m - T_0)}\right]^2 \tag{9}$$

$$t = B\left(\frac{V}{S}\right)^n \tag{10}$$

K_m Mould thermal conductivity

ρ_m Mould density

C_m Mould specific heat

a Geometric modulus (equal to $\frac{2 \cdot V}{S}$)

ρ_s Solid density

H Latent heat of solidification

T_m Casting temperature

T_0 Mould starting temperature

V Volume of the part ($V_{cylinder} = r \cdot \pi \cdot h$)

S Surface of the part in contact with the mould ($S_{cylinder} = 2 \cdot \pi \cdot r(r + h)$)

According to [39], $n = 2$ was assumed. Considering a cylindrical shape of the risers and a given height h_r, their radius could be calculated with Eq. (9) by rearranging Eq. (8), since the mould coefficient is equal for the casting part and the risers.

$$r_{\text{riser}} = \frac{2 \cdot h_{\text{r}} \cdot \sqrt{\frac{1.2 \cdot t}{B}}}{h_{\text{r}} - 2} \tag{11}$$

Assuming a 20 % longer solidification time for the risers compared to the casting part [40] and a safety margin of 4, the radius of the risers was set to 32 mm. The safety margin was defined based on foundry experience, the effort to produce as many defect-free parts as possible despite very low quantities and the placement of the risers in a cold zone.

To check the casting design, filling and solidification simulations were carried out afterwards with the use of ProCast (ESI Group, Paris, France). Force of gravity and the centrifugal force due to the rotation were applied.

4.3 Mould design

Due to the geometrical complexity of the part, the sand mould was manufactured using the Binder Jetting additive manufacturing method. This process allows sand moulds to be built with layers of bonded sand with a resolution of the sand grain size used ($\approx$ 100 µm). In this way, complex cavities and shapes are feasible. To have a good access to the neck of the risers and to avoid too thin cantilevered flanges, the parting line of the mould was defined as shown in Fig. 10. Depending on its placement, the moulding process could be conditioned and fragile parts of the mould left uncovered, increasing the probability of breakage.

In addition, solidification shrinkage must be considered, which occurs once the metal has solidified and cooled down. As a result, the dimensions of the mould and the dimensions of the part would differ, which is generally expressed as a linear shrinkage. Based on the aluminium sand casting process, a shrinkage of 1.2 % is assumed [41].

4.4 Post-processing

Post-processing of the cast part via turning and milling was required to compensate distortion and provide required surface quality for component interfaces. The nano-reinforced particles increased machinability and decreased typical aluminium flow chips. For balancing 12 M3 screw threads are created at the upper and lower section of the rim. Since this design was a proof of concept, it was assumed that a low balancing grade was acceptable.

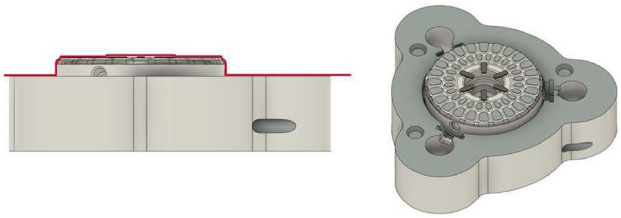

Fig. 10 Parting line of the mould

5 Vibration measurement

Since the strength of arising vibrations is a relevant aspect for the reliable operation of the rotor, micro-vibrations caused by the rotor were experimentally measured at different rotational speeds. For a qualitative analysis, three uniaxial acceleration sensors of the type PCB 333B50 were mounted onto the rotor stator. Figure 11 shows the measurement setup.

A mass transfer function was used for conversion from the measured accelerations into forces, which were related to resonance of the part. In this, dynamic resonance was caused by rotor imbalance or ball bearing, whereas static resonance were the component natural frequencies in the setup. Figure 12 displays dynamic and static resonance measurement results for rotations of 1000 RPM down to 0 RPM. A disc shaped calibration rotor was used at first. Here, also the

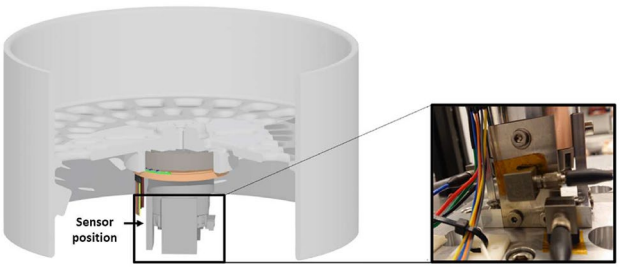

Fig. 11 Rotor vibration measurement setup

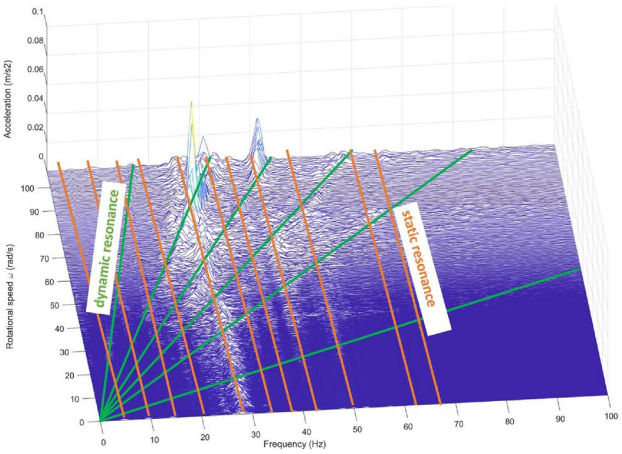

Fig. 12 Rotor vibration measurement results for rotation of 1000 RPM down to 0 RPM on the balanced rotor

static resonance shown in Fig. 12 existed. Consequently, static resonance related to test setup and the rotor mounting. It can be seen that the static resonance amplify also the dynamic resonances. Additionally, in operation three-point-balancing in one plane was conducted to reduce the disturbance amplitude. To reach the displayed static imbalance, a balancing mass of 30 g was necessary. The relatively high imbalance limited the allowable rotation rate as the bearings could not fully compensate the eccentric motion of the rotor. The electric motor air gap defined acceptable eccentric motion. The displayed disturbance amplitude value in Fig. 12 is insignificant as the transfer function is unknown.

6 Discussion

The development of the bio-inspired reaction wheel rotor design, manufactured as a sand mould cast part, was realised by performing different development steps. Each step is discussed in the following.

6.1 Bio-inspired design process

The abstraction and implementation of the bio-inspired design principles revealed some limitations. Although complex, filigree and hierarchical structures are usually found in diatoms, the abstracted rotor design appeared very rudimentary, caused by a high level of abstraction simplification. The manufacturing-related minimum material thickness of 7 mm prevented the use of bio-inspired structures like lattices or fractal combs. Those structures can be found in nature in a variety of forms and posses high mass saving potential among other mechanical benefits [42]. In addition, the assumption of an horizontal symmetric rotor adds up to the simplifications. Therefore, the present design could be considered as an optimised design with unexploited potential. This is in line with [43] who proposed that the success of a bio-inspired design mainly depends on the implementation of an analogy at an appropriate level of abstraction.

The unexploited mass saving potential is also apparent in the rotor performance according to occurring stresses. As the maximum stress is around 18 % lower than the yield strength, material of the rotor could be further reduced resulting in less mass and stresses closer to the maximum allowed value. Nevertheless, the mass distribution must still ensure the required mass moment of inertia, manufacturability and yield strength compliance.

Compared to the topology-optimised concept design of [11] and the simplified commercial reference model of [1], the bio-inspired design has to be critically evaluated, since its mass is 44 % higher. Although the inertia to mass ratio is about 19 % worse compared to the concept design, the performance in terms of energy density (+30 %) and inertia ratio (+27 %) shows significant improvements. In addition, the design is much more compact due to a smaller rotor diameter, even though the maximum rotor height is larger. Furthermore, the rotor inertia of the concept design is about 20 % lower and the design is highly simplified so that no structural interfaces for bearings, launch looks or similar structures were considered. Their implementation as well as an increase in inertia are accompanied by an increase in mass, so that the comparison to the concept design can only be considered to be of limited meaning.

The comparison with the commercial model does not have these limitations, since the same relevant characteristics as the fully functional initial component are represented, although it is simplified according to [1]. Identical to the concept design, the bio-inspired design is built more compactly. At approximately the same inertia and inertia ratio, the inertia to mass ratio is 34 % lower for the bio-inspired design. At the same time, the new design enables up to 67 % faster speeds and 85 % higher energy density. In addition, it must be considered that the bio-inspired design is made of aluminum, allowing for improved demisability, thus providing an advantage over the commercial stainless steel rotor.

The comparison with the commercial model is much more meaningful, despite the fact that the speed and angular momentum differ significantly. Therefore, it can be concluded that a similarly performing mass distribution was achieved (indicated by the inertia ratio) with a significantly higher energy density. A mass reduction and the implementation of a “lightweight” design could not be implemented to a large extent. The reason for this are the manufacturing restrictions. Since the material and the hybrid manufacturing approach are still at a development stage, the probability of comprehensive improvements is high, so that significantly lower material thicknesses could be produced. As a result, material could be reduced, especially in the centrally located, low stressed areas. This would have little effect on inertia, as this depends mainly on the rim of the rotor. In addition, the comb-like area could be replaced by finer patterns or lattices, which would save further mass. Based on these points, it can be seen that the design and approach offer the potential to make a lightweight, bio-inspired rotor design more likely in the future.

6.2 Material selection

An aluminium alloy was selected to allow fast burn up of the rotor during re-entry in the atmosphere and to benefit from higher specific energy density at lower rotor radii and high speeds. Despite taking into account the previously explained limitations of the mass saving potential of the bio-inspired design principles, the use of nano-reinforced aluminium did not seem to enable a significant advantage in terms of the analysed rotor properties. From materials perspective, higher

density materials, as the already in use Inconel 718, offer advantages in terms of rotor mass efficiency. Furthermore, an Inconel alloy would also allow higher mechanical stresses and enable further size reduction. In addition, Inconel has a higher fatigue strength. From a post-processing perspective, the nano-reinforced particles increased machinability and decreased typical aluminium flow chips which is beneficial.

6.3 Casting process

During the casting process, challenges were encountered that might have affected the casting and present opportunities for improvement. First, rotation has to been given to the mould as explained in 4.2. A rotating table was used and a speed of 1 RPM was applied to the system by hand. The main problem here was to align the center of rotation and the center of gravity of the mould, especially due to the weight of the assembly. Second, the pouring of the metal into the mould had to be fast enough to fill the whole part before it started solidifying. As the part is thin, the solidification of the molten alloy happened almost immediately. Third, due to complexity, the center area, where the feeder is attached, and the lock connections at the inside of the rim were cast as solid geometries without cavities. Therefore, the effort and complexity of the post-processing was significantly higher than if only the additional cast structures had to be removed.

In addition, the post-processing revealed that the casting quality is affected by generated pores with a diameter of about $0.5 - 1$ mm. Potential reasons are bad degassing, drags from the moulds or an improvable casting design, so that these factors need to be further considered to improve the outcome of the casting process.

As mentioned in the discussion about the bio-inspired design process, using lattice or fractal honeycomb structures, improvements in the rotor performance can be expected, but fabrication of these structures would require a reduction in the minimum material thickness. Alternatively, fabrication using additive manufacturing might be an option, although the advantages of a nano-reinforced material could then be lost and the possibility of manufacturing a larger amount of parts, which the casting process enables, would disappear.

6.4 Vibration measurement

In comparison to other mechanical parameters of the new rotor, no test on the commercial rotor was performed and accordingly no comparison was made. The aim of this measurement was to prove whether the frequency requirements were met.

The conducted measurements showed that the balancing process is critical to achieve low vibration emission. The detailed analysis of the casting deformations were essential for the post-processing to obtain low imbalance. As explained, the conducted measurement can only provide a qualitative evaluation of the rotor performance, due to the mass transfer function. This function is difficult to predict since it depends on all reaction wheel components and the mounting for measurement. For more accurate evaluation, the function should be determined via direct force measurements. In addition, modal analysis of the rotor showed that the measured resonance comes from measurement setup and not to the rotor itself. As a third point, the tested rotational speed should be increased up to the maximum speed of 7500 RPM, to draw conclusions about the entire range of operational speed.

7 Conclusion

In this work, a bio-inspired rotor design based on design principles of marine microorganisms and an algorithm-based workflow could be realised and manufactured as a proof of concept using nano-reinforced aluminium and sand mould casting. The new design represents an objective-fulfilling compact rotor for small to medium satellites, capable of high-speed spinning and good performance in terms of inertia ratio, energy density and natural frequency requirements. Regarding manufacturing, the hybrid process using additive manufacturing and casting has aroused as a useful method to manufacture complex structures with small cost and high efficiency, so that aluminium sand casting is a viable option when manufacturing lightweight, complex or optimised parts.

Future work might focus on the improvement of the casting process enabling the use of finer, more complex bio-inspired cellular structures to use more mass-saving potential of the shown process. Additional, in-depth casting FEM-simulations for improved casting design and validated mechanical and thermal performance of the concept, represent further, useful additions to the development process.

Acknowledgements The authors also acknowledge the support from their direct project partners of the OASIS project, the University of Patras (UoP), BLUMORPHO (BLU), SISTEPLANT (SIS) and the Commissariat à l'énergie atomique et aux énergies alternatives (CEA), and would like to thank them for a good and fruitful collaboration during the development, evaluation and simulation of the proposed proof of concept. Additionally the authors would like to thank ZARM Technik AG and the University Bremen for providing the use case and support during LOBSTER.

Author Contributions NK: writing—original draft, writing section bio-inspired design process, its discussion and the conclusion— review and editing other sections. NG: concept idea, writing—original draft, writing sections application constraints, vibration measurement, discussion on material selection and vibration measurements—review and editing other sections. AJ: advanced manufacturing process and writing, review and editing other sections. IL: bio-inspired design process and review/editing, advanced manufacturing process and writing, review

and editing other section. SP: review finite element analysis. ST: review finite element analysis.

Funding Open Access funding enabled and organized by Projekt DEAL. The LOBSTER use case, as part of the OASIS project, has received funding from the European Union's Horizon 2020 research and innovation programme under grant agreement No 814581 (related to the OASIS project participants AWI, TEC, UoP, CEA, SIS and BLU). The assessment of ZARM Technik AG and the University Bremen is part of Project RIMoNA (Reaction wheel rotor with Integrated MagNetic bearing using Additive manufacturing) which has been funded by ESA Contract 4000124501/18/NL/MH/mg.

Data availability Further data as well as code can be provided if a request is sent to the corresponding authors.

Declarations

Conflict of interest The authors declare that there is no conflict of interest.

References

1. Park, S.H., Mischler, S., Leyland, P.: Re-entry analysis of critical components and materials for design-for-demise techniques. Adv. Space Res. **68**(1), 1–24 (2021)
2. Spel, M., Dumon, J., Constant, E., Van Hauwaert, P., Galera, S., Annaloro, J.: Demisability study of industrial test cases with the spacecraft-oriented code pampero. In: Proceedings of 8th European Conference on Space Debris (2021)
3. Klein, B.: Leichtbau-Konstruktion, 10th edn. Springer Vieweg, Cham (2013)
4. Arslan, M.A.: Flywheel geometry design for improved energy storage using finite element analysis. Mater. Des. **29**, 514–518 (2008)
5. Strößenreuther, F.: Machbarkeitsstudie und Konzept einer stationären Schwungradanalge zur dezentralen, verbraucherorientierten Energiespeicherung. Diplomarbeit, Institut für Dampf- und Gasturbinen, Rheinisch-Westfälischen Technischen Hochschule Aachen (1996)
6. Pedrolli, L., Zanfei, A., Ancelotti, S., Fontanari, V., Benedetti, M.: Shape optimization of a metallic flywheel using an evolutive system method: design of an asymmetrical shape for mechanical interface. Proc. Inst. Mech. Eng. Part C **232**, 217–230 (2016)
7. Kress, G.R.: Shape optimization of a flywheel. Struct. Multidiscip. Optim. **19**, 74–81 (2000)
8. Jiang, L., Wu, C.W.: Topology optimization of energy storage flywheel. Struct. Multidiscip. Optim. **55**, 1917–1925 (2017)
9. Jiang, L., Zhang, W., Ma, G.J., Wu, C.W.: Shape optimization of energy storage flywheel rotor. Struct. Multidiscip. Optim. **55**, 739–750 (2017)
10. Kale, V., Thomas, M., Secanell, M.: On determining the optimal shape, speed, and size of metal flywheel rotors with maximum kinetic energy. Struct. Multidiscip. Optim. **64**(3), 1481–1499 (2021)
11. Lottes, L. M., Kaiser, N., Goossens, N., Oelze, H. W., Braxmaier, C.: TOMARES-topology optimization of an additive manufactured reaction flywheel designed for an earth-observation satellite. CEAS Space J. **13**, 521–532 (2021)
12. Farzaneh, H.H., Lindemann, U.: A Practical Guide to Bio-inspired Design, 1st edn. Springer Vieweg, Heidelberg (2019)
13. Müller, R., Abaid, N., Boreyko, J.B., Fowlkes, C., Goel, A.K., Grimm, C., Jung, S., Kennedy, B., Murphy, C., Cushing, N.D., Han, J.P.: Biodiversifying bioinspiration. Bioinspir. Biomim. **13**(5), 053001 (2018)
14. VDI 6220 Blatt 1: Bionik-Konzepte und Strategie (2012)
15. Kull, U.: Vegetationsverhältnisse in Trockengebieten und die Leichtbauweise von Pflanzen. Jh. Ge. Naturkde. Wüm. **145**, 5–33 (1990)
16. Round, F.E., Crawford, R.M., Mann, D.G.: The Diatoms - Biology and Morphology of the Genera. Cambridge University Press, Cambridge (1990)
17. Hamm, C.: The evolution of advanced mechanical defenses and potential technological applications of diatom shells. J. Nanosci. Nanotechnol. **5**(1), 108–119 (2005)
18. Hamm, C., Smetacek, V.: Armor: why, when and how? In: Falkowski, P., Knoll, A. (eds.) The Evolution of Aquatic Photoautotrophs. Elsevier, Amsterdam (2007)
19. Maier, M., Siegel, D., Thoben, K.-D., Niebuhr, N., Hamm, C.: Transfer of natural micro structures to bionic lightweight design proposals. J. Bionic Eng. **10**(4), 469–478 (2013)
20. Hundertmark, C., Tinter, R., Ortelt, M., Hauser, M.J.B.: Diatom-inspired plastic deformation elements for energy absorption in automobiles. J. Bionic Eng. **12**(4), 613–623 (2015)
21. Heinrichs, A., Frank, P., Siegel, D., Frank, M.: Bionische Entwicklung einer additiv gefertigten A-Säulen-Verstärkung. Lightweight Des. **10**, 74–81 (2017)
22. Hamm, C., Siegel, D., Niebuhr, N., Jurkojc, P., von der Hellen, R.: Offshore foundation based on the ELiSE method. In: Hamm, C. (ed.) Evolution of Lightweight Structures - Biologically-Inspired Systems, vol. 6, pp. 195–206. Springer, Dordrecht (2015)
23. Andresen, S.: Impact of bio-inspired structural irregularities on plate eigenfrequencies. In: Sapountzakis, E., Banerjee, M., Biswas, P., Inan, E. (eds.) Proceedings of the 14th International Conference on Vibration Problems. Lecture Notes in Mechanical Engineering, 14th International Conference on Vibration Problems, Singapore. Springer, Cham (2021)
24. Andresen, S., Bäger, A., Hamm, C.: Eigenfrequency maximisation by using irregular lattice structures. J. Sound Vib. **465**, 115027 (2020)
25. Andresen, S.: Optimizing the PETRA IV girder by using bio-inspired structures. In: Mechanical Engineering Design of Synchrotron Radiation Equipment and Instrumentation (MEDSI), Paris, France, 25–29 June (2018)
26. Hamm, C., Möller, S.: ELiSE: an integrated, holistic bionic approach to develop optimized lightweight solutions for engineering, architecture and design. In: Hamm, C. (ed.) Evolution of Lightweight Structures. Biologically-Inspired Systems, vol. 6, pp. 183–194. Springer, Dordrecht (2015)
27. Lal, B., de la Rosa Blanco, E., Behrens, J.R., Corbin, B.A., Green, E.K., Picard, A.J., Balakrishnan, A.: Global Trends in Small Satellites. Institute for Defense Analyses. Science and Technology Policy Institute. IDA Paper P-8638 (2021)

28. Borque Gallego, G.: Performance and micro-vibrations in magnetic bearings for space actuators. PhD thesis doctor of science. EPFL (2021)
29. Ehinger, M., Kärräng, P.: Assessment of design for demise approaches for reaction wheels. Clean space industrial days. https://indico.esa.int/event/234/contributions/4042/attachments/3052/3796/2018CSID_PKaerraengEhinger_DemisabilityAnalysisofReactionWheels.pdf (2018)
30. Helms, M., Vattam, S.S., Goel, A.K.: Biologically inspired design: process and products. Des. Stud. **30**(5), 606–622 (2009)
31. Pohl, G., Nachtigall, W.: Biomimetics for Architecture and Design Nature Analogies Technology, 1st edn. Springer International Publishing, Cham (2015)
32. Potapova, M., Veselá, J., Smith, C., Minerovic, A., Aycock, L. (Editors): Diatom New Taxon File at the Academy of Natural Sciences (DNTF-ANS), Philadelphia. http://dh.ansp.org/dntf (2022). Retrieved 15 July 2022
33. MIDACO-Solver. http://www.midaco-solver.com/ (2022). Retrieved 10 July 2022
34. European cooperation for space standardization (ECSS): ECSS-E-ST-32-10 - structural factors of safety for spaceflight hardware. ECSS Secretariat, ESA-ESTEC, Requirements and Standards Division, Noordwijk, The Netherlands (2009)
35. Ullman, D.G.: The Mechanical Design Process, 4th edn. McGraw-Hill Series in Mechanical Engineering, McGraw Hill (2009)
36. Nandiyanto, A.B.D., Zaen, R., Oktiani, R.: Working volume in high-energy ball-milling process on breakage characteristics and adsorption performance of rice straw ash. Arab. J. Sci. Eng. **43**(11), 6057–6066 (2018)
37. Karbalaei Akbari, M., Baharvandi, H.R., Mirzaee, O.: Fabrication of nano-sized Al2O3 reinforced casting aluminum composite focusing on preparation process of reinforcement powders and evaluation of its properties. Compos. B. Eng. **55**, 426–432 (2013)
38. Campbell, J.: Flow. In: Complete casting handbook - Metal Casting Processes, Metallurgy, Techniques and Design, 2nd edn., pp. 91–134. Butterworth-Heinemann, Oxford (2015)
39. Askeland, D.R., Wright, J.W.: Essentials of Materials Science and Engineering, 3rd edn. CENGAGE Learning Custom Publishing, Boston (2013)
40. Campbell, J.: The 10 rules for good casting. In: Complete Casting Handbook - Metal Casting Processes, Metallurgy, Techniques and Design, 2nd edn., pp. 535–638. Butterworth-Heinemann, Oxford (2015)
41. Campbell, J.: Dimensional accuracy. In: Complete Casting Handbook - Metal Casting Processes, Metallurgy, Techniques and Design, 2nd edn., pp. 893–926. Butterworth-Heinemann, Oxford (2015)
42. McNulty, T., Bhate, D., Zhang, A., Kiser, M. A., Ferry, L., Suder, A., Bhattacharya, S., Boradkar, P.: A framework for the design of biomimetic cellular materials for additive manufacturing. In: 2188-2200. 28th Annual International Solid Freeform Fabrication Symposium - An Additive Manufacturing Conference, SFF 2017, Austin, United States (2020)
43. Yen, J., Weissburg, M.: Perspective on biologically inspired design: introduction to the collected contributions. Bioinspir. Biomim. **2**, E01 (2007)